Journal of Electroceramics, 11, 73–79, 2003

Electrical Conductivity of Cu-Doped ZnO and its Change with Hydrogen Implantation

ZHEN ZHOU,[1]* K. KATO,[1] T. KOMAKI,[1] M. YOSHINO,[1] H. YUKAWA,[1] M. MORINAGA[1] & K. MORITA[2]

[1]*Department of Materials Science and Engineering, Graduate School of Engineering, Nagoya University, Furo-cho, Chikusa-ku, Nagoya, Aichi, 464-8603, Japan*

[2]*Department of Nuclear Engineering, Graduate School of Engineering, Nagoya University, Furo-cho, Chikusa-ku, Nagoya, Aichi, 464-8603, Japan*

Submitted March 11, 2003; Revised June 24, 2003; Accepted November 7, 2003

Abstract. The doping effects of Cu on the electrical conductivity of ZnO were studied in the simple binary system through the ac impedance spectroscopy. The Cu doping decreased the electrical conductivity of ZnO by several orders of magnitude. The Cu doping decreased the electrical conductivity of ZnO both in the grain and in the grain boundary. Hydrogen was introduced into the Cu-doped ZnO specimens by the ion implantation technique. The electrical conductivity of the hydrogen-implanted layer increased by about 9 orders of magnitude at most. The mechanism for such a hydrogen effect was also discussed.

Keywords: ZnO, electrical conductivity, hydrogen, grain boundaries, impedance

Introduction

The wide-band-gap oxide, ZnO, is intrinsically *n*-type semiconductor. It has been widely used in piezoelectric transducers, varistor, gas sensor, catalyst, and transparent conducting films [1–5]. If the *p*-type ZnO is achieved, it can be used for optoelectronic applications. So recently it has attracted many researchers' interests to explore the possibility of achieving the *p*-type ZnO theoretically and experimentally. A potential candidate for a *p*-type dopant is Cu [6–8]. Cu is well known as an acceptor impurity in *n*-type ZnO, and has significant effects on the electrical and optical properties of ZnO [9–11]. Kutty et al. reported the varistor properties of polycrystalline ZnO:Cu [12], and then Cu was extensively studied as an important additive in the ZnO-based varistors [13, 14]. The role of Cu in the ZnO-based varistors is different from other dopants such as Mn, Co and Bi, Pr, etc. [14–21]. It is important to understand the effects of Cu in a fundamental manner. There were some reports on the Cu doping in the ZnO varistor, but the effects of Cu on the grain and grain boundary of ZnO still remain unclear. In the present experiment simple binary ZnO systems were used to investigate the effect of Cu on the electrical conductivity both in the grain and in the grain boundary of ZnO through the ac impedance spectroscopy.

Zinc oxide exhibits strong *n*-type conductivity with the electrons to move in the conduction band as charge carriers. In spite of extensive investigations, the source of such conductivity is still in debate. For many years the *n*-type conductivity has traditionally been attributed to native defects [22, 23]. However, a recent first-principles investigation has revealed that none of the native defects may exhibit the characteristics consistent with a high-concentration shallow donor, but instead hydrogen is a promising candidate for the impurity causing the *n*-type conductivity in ZnO [24]. Experimental indications for hydrogen to behave as a donor in ZnO were reported in 1950's [25], but no one paid attention to those results for many years. Recently, many researchers' interests have been focusing on the hydrogen behavior in ZnO [26–37]. There seems no argument on the shallow donor behavior of hydrogen in ZnO, but there are still debates on whether

*To whom all correspondence should be addressed. E-mail: shushin@silky.numse.nagoya-u.ac.jp

hydrogen is the real source of *n*-type conductivity in ZnO [37]. The real source of *n*-type conductivity in ZnO might be more complicated than expected. There is the possibility that the *n*-type conductivity of ZnO is caused by some intrinsic defect complexes or H-defect complexes. So it is still important to deeply study the behavior of hydrogen in ZnO, such as the interaction between hydrogen and intrinsic defects or extrinsic impurities. Zwingel studied the Cu-H centers in ZnO by EPR spectra in 1975 [38]. In the present investigation hydrogen was introduced into the Cu-doped ZnO by the ion implantation method, and the effects of hydrogen on the electrical conductivity of the Cu-doped ZnO were investigated.

Experimental

The wet chemical method [39, 40] was used for the preparation of the undoped and Cu-doped ZnO powders. In the starting solution the compositional ratio of copper to zinc was controlled to 100, 400, 700 and 1000 ppm, respectively. The structure of the powder was analyzed with an X-ray diffractometer (XRD, RAD-IIC, Rigaku Co., Japan) using the Cu Kα radiation, and the grain size of the powder was analyzed by using a laser particle analyzer (LA-920, HORIBA, Japan).

The above ZnO powders were consolidated into the disk-shaped specimens with 1.2 cm in diameter and 2–2.5 mm in thickness by the uniaxial pressing at 30 MPa in a mold, and then isostatically pressed at 150 MPa. Specimens were placed in crucibles and sintered in a muffle furnace, where the temperature was controlled through programs. The sintering condition was kept as follows; specimens were kept at 1000°C for 2 h, heated up to 1350°C at the speed of 3°C/min and then kept for 3 h at this temperature, and subsequently taken out of the furnace and cooled down to room temperature in air.

Sintered specimens were cut and polished into the shape of $0.8 \times 0.8 \times 0.03$ cm, and were ultrasonically cleaned. The specimens were annealed at 1000°C for 24 h to eliminate the surface mechanical damages during the polishing. The In-Ga alloy was used to make electrodes for the electrical measurements. The ac impedance was measured with impedance analyzers (3535 LCR HiTESTER and 3522-50 LCR HiTESTER, HIOKI, Japan). The modulus of complex impedance $|Z * (\omega)|$ and phase angle $\theta(\omega)$ were recorded from the frequency 1 MHz to 1 Hz. The impedance spectra were simulated using the software ZView (Scribner Associates, Inc.) to separate useful parameters. All the electrical measurements were conducted at room temperature.

Hydrogen was introduced into the above Cu-doped ZnO thin flake using the ion implantation technique (ULVAC-PHI Incorporated, Japan), after the electrical measurements. The H_2^+ ions were implanted into ZnO specimen using a 5 keV ion gun and the implantation dose was 1.44×10^{17} ions/cm^2. The contents of hydrogen in the specimen were measured by the means of elastic recoil detection analysis (ERD, AN-2500, Nissin High Voltage Co., Ltd., Japan) before and after the H_2^+ ions implantation. The surfaces of the ZnO specimens were observed before and after hydrogen implantation using a scanning electron microscopy (SEM, S-3500H, Hitachi, Japan).

Results

According to the X-ray diffraction analysis, all the undoped and Cu-doped ZnO specimens had the Wurtzite-type structure, and no formation of new phase could be found in any Cu-doped ZnO specimens. All the sintered specimens had the apparent density over 5.4 gcm^{-3}, higher than 95% of the theoretical value, 5.67 gcm^{-3}.

The ac impedance spectra of the undoped and Cu-doped ZnO specimens are shown in Fig. 1. All the spectra contain a single arc, but the arc has a non-zero intersection with the real axis in the high frequency region. It is labeled as R_0 in the equivalent circuit in Fig. 2. The resistance R_0 is attributed to the ZnO grains, in accordance with the generally accepted view. The intersection between the arc and the real axis in the low frequency region represents the total dc resistance of the sample. R_1CPE_1 is attributed to the response of the grain boundary region of ZnO. In some ZnO varistor studies this part was divided into two parts: intergranular layer and interface between grain and intergranular layer [41, 42]. Here capacitance elements are represented by a constant phase element (CPE) with an admittance, $Y = Y_0(j\omega)^n$, where Y_0 is the admittance module, ω is the angular frequency and n is the frequency power factor of the CPE, which can indicate the level of the depression of the semicircle in the impedance spectrum. The experimental impedance data were well simulated using this equivalent circuit and the above parameters were separated.

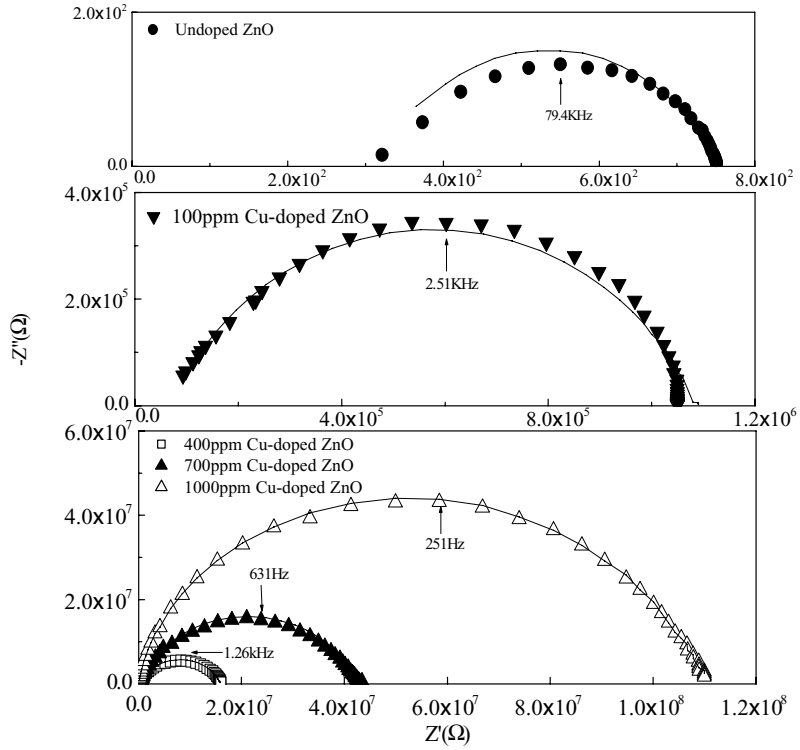

Fig. 1. Impedance spectra of Cu-doped ZnO specimens with different Cu doping content (the solid lines denote the fitting results).

The simulated results were shown as solid lines in Fig. 1. The parameters R_0 and R_1 were used to estimate the grain and grain boundary electrical conductivity. The results are summarized in Fig. 3, where σ_g is the electrical conductivity of the grain, σ_{gb} is the electrical conductivity due to the grain boundary region, and σ is the total electrical conductivity.

It can clearly be seen from Fig. 3 that the electrical conductivity of the Cu-doped ZnO is much lower than that of the undoped ZnO. The electrical conductivity of even the 100 ppm Cu-doped ZnO specimen was about 3 orders of magnitude lower than that of the undoped ZnO. With the increase of the doped Cu content, the electrical conductivity decreased gradually. The 1000 ppm Cu-doped ZnO had the electrical conductivity 5 orders of magnitude lower than that of the undoped ZnO.

As shown in Fig. 3, the grain and grain boundary electrical conductivity of ZnO both changed with the doped Cu content. It can be seen from this figure that there was much greater difference between the grain and grain boundary electrical conductivity for all the Cu-doped ZnO specimens than the undoped ZnO specimen. With the increase of the doped Cu content beyond 100 ppm, the decrease of the grain electrical conductivity was not very significant, while the electrical conductivity of the grain boundary decreased by 2 orders of magnitude. The total resistance of the Cu-doped ZnO specimens was mainly caused by the grain boundary.

In the present investigation, the above ZnO specimens were further used for the study of the doping effect of hydrogen on the electrical conductivity of ZnO. The sintered specimen was thinned down to about 0.3 mm, and then, the H_2^+ implantation was applied to the specimen surface.

Figure 4 is the result of the ERD analysis for the 1000 ppm Cu-doped ZnO specimen before and after the H_2^+ implantation. It was found from this figure that hydrogen really existed in the Cu-doped ZnO specimens

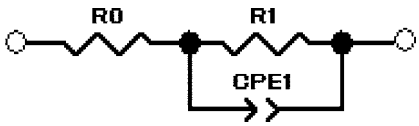

Fig. 2. Equivalent circuit for the simulation of impedance spectra.

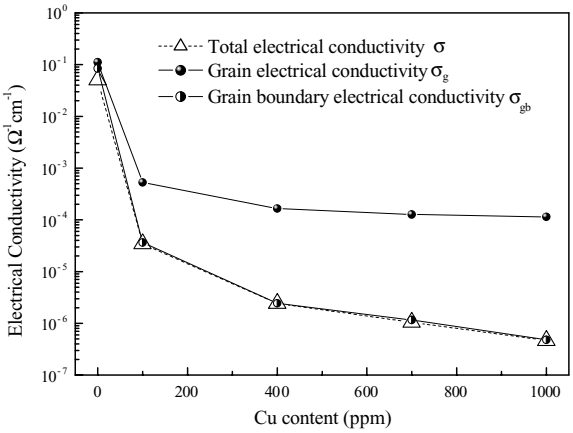

Fig. 3. Changes in the grain and grain boundary electrical conductivity of ZnO with Cu content.

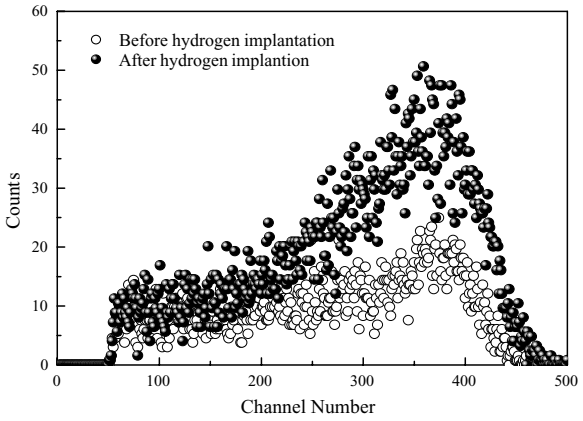

Fig. 4. ERD analysis for the Cu-ZnO specimen before and after hydrogen implantation.

even before the H_2^+ implantation. Also, the counts of hydrogen ions increased apparently after the H_2^+ implantation. Hydrogen was also detected by ERD in the undoped ZnO, and its counts increased after hydrogen implantation, but the counts were lower than that of the Cu-doped ZnO both before and after hydrogen ion implantation [39, 43].

The ac impedance spectra of all the specimens after the H_2^+ implantation were also measured, but in all the spectra the single arc disappeared, so we could only estimate the dc electrical conductivity from the impedance measurements. According to the hydrogen stopping power [44], it can be calculated that the H_2^+ ions with the energy 5keV can be implanted into the

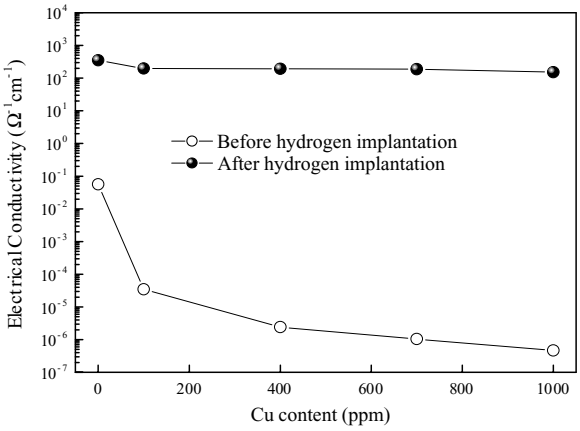

Fig. 5. Changes of the electrical conductivity of ZnO specimens before and after hydrogen implantation.

depth of about 200 nm in the ZnO specimens. So the electrical conductivity in the hydrogen-implanted layer can be estimated, shown in Fig. 5. From Fig. 5 it can be seen that after hydrogen implantation there is no such apparent difference among the samples in the electrical conductivity as before hydrogen implantation. The electrical conductivity of the most resistive 1000 ppm Cu-doped ZnO increased from $4.6\times10^{-7}\Omega^{-1}$ cm^{-1} to 1.5×10^{2} Ω^{-1} cm^{-1} after the hydrogen implantation. This result approaches to that of Kohiki et al. [35].

Discussion

It is well known that the Cu^+ ions are substituted for Zn^{2+} ions in the ZnO lattice and behave as an acceptor-type impurity. Since the extrinsic donor is absent in the Cu-doped ZnO specimen, and Cu'_{Zn} has to be compensated by either the hole or the intrinsic donor to keep the electroneutrality, the grain electrical conductivity of the *n*-type ZnO semiconductor decreased greatly by the Cu doping.

The Cu doping had more significant effect on the electrical conductivity in the grain boundary of ZnO in the present experimental results. The width of the space charge region can be expressed by Eq. (1). In Eq. (1), W is the width of the space charge region, ε is the dielectric constant, q is the elementary charge, and V is the total potential drop across the space charge region, and N_D and N_A is the concentration of the donors and the acceptors, respectively. V is often defined as

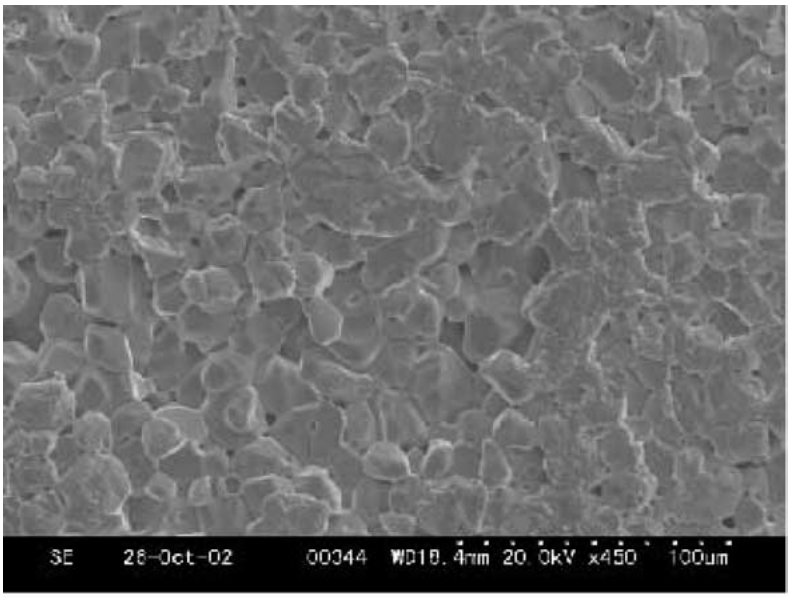

(a)

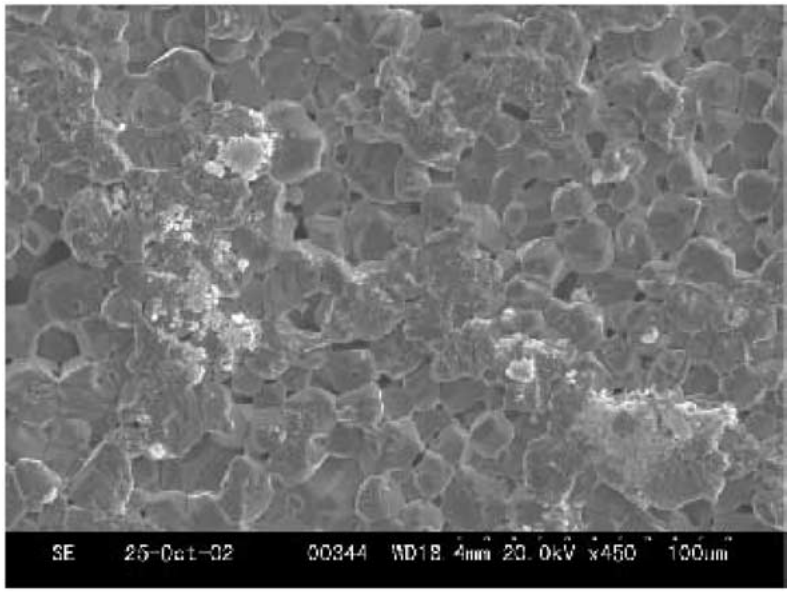

(b)

Fig. 6. SEM micrographs for the surface of undoped ZnO specimen before hydrogen implantation (a) and after hydrogen implantation (b).

the built-in potential minus the applied potential, $V = V_{(\mathrm{BI})} - V_{(A)}$.

$$W = \left(\frac{2\varepsilon V}{q(N_D - N_A)} \right)^{1/2} \tag{1}$$

We can see from Eq. (1) that the net donor concentration influences the width of the space charge region. The Cu doping in ZnO decreases the concentration of the intrinsic donor, and results in a larger space charge region, so it is easily to understand the fact that the

grain boundary of the Cu-doped ZnO is much more resistive than the grain. The introduction of Cu into ZnO decreased the net donor concentration sharply, so the difference in the electrical conductivity between the undoped ZnO and the Cu-doped ZnO were enormous, but among the Cu-doped ZnO specimens the difference was not so striking with the increase of the Cu content.

It was found from Fig. 4 that hydrogen really existed in the Cu-doped ZnO specimens even before the H_2^+ implantation. This result can prove that hydrogen is a very plausible impurity unintentionally incorporated into ZnO in the preparation process. However, Ip et al. [37] found that hydrogen exhibited a very rapid diffusion in ZnO when incorporated by plasma exposure, and all of the plasma-incorporated hydrogen could be removed from the ZnO by annealing at $>500^\circ$C. So the authors questioned the possibility of hydrogen as the dominant shallow donor in as-grown ZnO, which was experienced the high temperature preparation process. This is not consistent with the present results. In the experiments of Ip et al. [37] ZnO single crystal was used, and they also found that the thermal stability was somewhat higher due to trapping at residual damage, when the hydrogen was incorporated by direct implantation. There is the possibility that the intrinsic defects and extrinsic impurities could affect the behavior of hydrogen in ZnO. Detailed experiments and some calculations are needed to investigate whether there are the effects of the intrinsic defects and extrinsic impurities on the existence of hydrogen in ZnO. There is the possibility that the *n*-type conductivity of ZnO is caused by some defect complexes or H-defect complexes.

It can be seen from Fig. 6 that there was some damage in the surface of the ZnO specimen after the hydrogen implantation. We believe that the damage of the surface is not the main reason for the increase in the electrical conductivity, because we also found that, when He^+ ions were implanted into the ZnO specimen, there were no apparent changes in the electrical conductivity.

It has been theoretically predicted that hydrogen forms a shallow donor level in ZnO [24]. The implanted H_2^+ ions move readily from the interstitial site to the neighboring oxygen site and forms OH ions in the form of $(O_oH_i)^\bullet$. Here O_o, H_i and $^\bullet$ represent the O atom on the oxygen lattice site, H atom in the interstitial site, and the singly ionized donor, respectively. The $(O_oH_i)^\bullet$ unit can be regarded as a new type of donor delivering an electron into the conduction band, which can turn the oxygen into a sort of doping element. In ZnO the Cu^+ ion behaves as an acceptor-type impurity. When more hydrogen ions were introduced into ZnO by the implantation, the formation of the above $(O_oH_i)^\bullet$ units will be enhanced as donors. The donor introduced by hydrogen will compensate the Cu'_{Zn}, and then the electrical conductivity will increase greatly.

The hydrogen introduced into ZnO acts as a shallow donor, so the net donor concentration in ZnO increases, and the width of the space charge region will decrease according to Eq. (1). As a result, the resistivity of the grain boundary will also decrease greatly. In our experiments the large arc in the impedance spectra, which indicates the conduction process in the grain boundary of the Cu-doped ZnO, disappeared after the hydrogen ion implantation. This is consistent with the above explanation.

Conclusions

The electrical conductivity was much lower in the Cu-doped ZnO than in the undoped ZnO. As the doped Cu content increased from 100 ppm to 1000 ppm, the electrical conductivity decreased gradually. There was also much larger difference between the grain and the grain boundary electrical conductivity for all the Cu-doped ZnO. With the increase of the doped Cu content beyond 100 ppm, the decrease of the grain electrical conductivity was not very significant, whereas the electrical conductivity of the grain boundary decreased by 2 orders of magnitude. The Cu^+ ion substituted for Zn^{2+} ion in the ZnO could behave as an acceptor-type impurity.

Hydrogen was introduced into the Cu-doped ZnO by the ion implantation technique. According to the ERD measurement results, the counts of hydrogen increased obviously after the H_2^+ implantation. As a result, the electrical conductivity of the specimens increased greatly after the H_2^+ implantation. The electrical conductivity of the hydrogen-implanted layer increased by about 9 orders of magnitude at most in this experiment. When hydrogen was introduced into ZnO, the formation of the $(O_oH_i)^\bullet$ units was probably enhanced and these units operated as the donors, so that the electrical conductivity increased greatly, in agreement with the present experiments.

Acknowledgments

This study was supported by a Grant-in-Aid for Scientific Research from the Ministry of Education, Culture, Sports, Science and Technology of Japan. One of the

authors (Zhen Zhou) thanks the financial support from the Japan Society for the Promotion of Science (JSPS).

References

1. D.C. Look, *Mater. Sci. Eng*., **B80**, 383 (2001).
2. T.K. Gupta, *J. Am. Ceram. Soc*., **77**(7), 1817 (1990).
3. M.E.V. Costa, P.Q. Mantas, and J.L. Baptista, *Sens. Actuator*, **B26/27**, 312 (1995).
4. D. Scarano, S. Bertarione, G. Spoto, A. Zecchina, and C.O. Arean, *Thin Solid Films*, **400**, 50 (2001).
5. B. Ismail, M. Abaab, and B. Rezig, *Thin Solid Films*, **383**, 92 (2001).
6. P. Fons, K. Nakahara, A. Yamada, K. Iwata, K. Matsubara, H. Takasu, and S. Niki, *Phys. Stat. Sol.*, **229**(2), 849 (2002).
7. P. Fons, A. Yamada, K. Iwata, K. Matsubara, S. Niki, K. Nakahara, and H. Takasu, *Nucl. Instrum. Methods Phys. Res. B*., **199**, 190 (2003).
8. S.-T. Jun and G.M. Choi, *J. Am. Ceram. Soc.*, **81**(3), 695 (1998).
9. R.E. Dietz, H. Kamimura, M.D. Sturge, and A. Yariv, *Phys. Rev*., **132**, 1559 (1963).
10. A. Hausmann, B. Schallenberger, and R. Roll, *Z. Phys.*, **B34**, 129 (1979).
11. Y. Kanai, *Jpn. J. Appl. Phys*., **30**(4), 703 (1991).
12. T.R.N. Kutty and N. Raghu, *Appli. Phys. Lett*., **54**(18), 1796 (1989).
13. B.-S. Chiou and M.-C. Chung, *J. Am. Ceram. Soc.*, **75**(12), 3363 (1992).
14. J.V. Bellini, M.R. Morelli, and R.H.G.A. Kiminami, *J. Mater. Sci.-Mater. Electron*., **13**, 485 (2002).
15. K. Mukae, K. Tsuda, and I. Nagasawa, *Jpn. J. Appl. Phys*., **16**(8), 1361 (1977).
16. H.H. Hoon and C.P. Ling, *Mater. Chem. Phys*., **9347**, 1 (2002).
17. J. Han, P.Q. Mantas, and A.M.R. Senos, *J. Eur. Ceram. Soc*., **21**, 1883 (2001).
18. J. Han, A.M.R. Senos, and P.Q. Mantas, *J. Eur. Ceram. Soc*., **22**, 1653 (2002).
19. J. Han, A.M.R. Senos, and P.Q. Mantas, *J. Eur. Ceram. Soc*., **19**, 1003 (1999).
20. J. Han, A.M.R. Senos, and P.Q. Mantas, *Mater. Chem. Phys*., **75**, 117 (2002).
21. J. Han, P.Q. Mantas, and A.M.R. Senos, *J. Eur. Ceram. Soc*., **22**, 49 (2002).
22. D.C. Look, J.W. Hemsky, and J.R. Sizelove, *Phys. Rev. Lett*., **82**, 2552 (1999).
23. Y. Sun, P. Xu, C. Shi, F. Xu, H. Pan, and E. Lu, *J. Electron. Spectrosc. Relat. Phenom*., **114–116**, 1123 (2001).
24. C.G. Van de Walle, *Phys. Rev. Lett*., **85**, 1012 (2000).
25. D.G. Tomas and J.J. Lander, *J. Chem. Phys*., **25**, 1136 (1956).
26. D.M. Hofmann, A. Hofstaetter, F. Leiter, H. Zhou, F. Henecker, B.K. Meyer, S.B. Orlinskii, J. Schmidt, and P.G. Baranov, *Phys. Rev. Lett*., **88**, 045504-1 (2002).
27. D.C. Look, *Mater. Sci. Eng*., **B80**, 383 (2001).
28. C.S. Han, J. Jun, and H. Kim, *Appli. Surf. Sci*., **175/176**, 567 (2001).
29. N. Ohashi, T. Ishigaki, N. Okada, T. Sekiguchi, I. Sakaguchi, and H. Haneda, *Appli. Phys. Lett*., **80**, 2869 (2002).
30. S.F. Cox, E.A. Davis, S.P. Cottrell, P.J. King, J.S. Lord, J.M. Gil, H.V. Alberto, R.C. Vilão, J. Piroto Duarte, de Campos N. Ayres, A. Weidinger, R.L. Lichti, and S.J. Irvine, *Phys. Rev. Lett*., **86**, 2601 (2001).
31. M. Arita, H. Konishi, K. Matsuda, M. Masuda, and Y. Hayashi, *Mater. Trans*., **43**(5), 1142 (2002).
32. Y.-S. Kang, H.-Y. Kim, and J.-Y. Lee, *J. Electrochem. Soc*., **147**(12), 4625 (2000).
33. S.J. Baik, J.H. Jang, C.H. Lee, W.Y. Cho, and K.S. Lim, *Appli. Phys. Lett.,* **70**, 3516 (1997).
34. C.G. Van de Walle, *Phys. B*, **308/310**, 899 (2001).
35. S. Kohiki, M. Nishitani, T. Wada, and T. Hirao, *Appli. Phys. Lett*., **64**(21), 2876 (1994).
36. N. Ohashi, T. Ishigaki, N. Okada, H. Taguchi, I. Sakaguchi, S. Hishita, T. Sekiguchi, and H. Haneda, *J. Appl. Phys*., **93**(10), 6386 (2003).
37. K. Ip, M.E. Overberg, Y.W. Heo, D.P. Norton, S.J. Pearton, C.E. Stutz, B. Luo, F. Ren, D.C. Look, and J.M. Zavada, *Appl. Phys. Lett*., **82**(3), 385 (2003).
38. D. Zwingel, *Phys. Stat. Sol*. (b), **67**, 507 (1975).
39. Z. Zhou, K. Kato, T. Komaki, M. Yoshino, H. Yukawa, M. Morinaga, and K. Morita, *J. Eur. Ceram. Soc*., **24**(1), 139 (2004).
40. M. Takehana, T. Nishino, K. Sugawara, and T. Sugawara, *Mater. Sci. Eng*., **B41**, 186 (1996).
41. M. Matsuura and H. Yamaoki, *Jpn. J. Appl. Phys*., **16**(7), 1261 (1977).
42. M. Andres-Verges and A.R. West, *J. Electroceramics*, **1**(2), 125 (1997).
43. Z. Zhou, K. Kato, T. Komaki, M. Yoshino, H. Yukawa, and M. Morinaga, *Int. J. Hydrogen Energy* **29**(3), 323 (2004).
44. H.H. Andersen and J.F. Ziegler, Hydrogen Stopping Powers and Ranges in all Elements (Wiley, New York, 1987).